Oxidation of 5-hydroxymethylfurfural with a novel aryl alcohol oxidase from *Mycobacterium* sp. MS1601

Mahmoud Sayed,[1,2] Yasser Gaber,[3,4] Fredrik Junghus,[1] Eric Valdés Martín,[1,†] Sang-Hyun Pyo[1] and Rajni Hatti-Kaul[1,*]

[1]*Division of Biotechnology, Department of Chemistry, Center for Chemistry and Chemical Engineering, Lund University, Lund, SE-22100, Sweden.*

[2]*Department of Botany and Microbiology, Faculty of Science, South Valley University, Qena, 83523, Egypt.*

[3]*Department of Microbiology and Immunology, Faculty of Pharmacy, Beni-Suef University, Beni-Suef, 62511, Egypt.*

[4]*Department of Pharmaceutics and Pharmaceutical Technology, Faculty of Pharmacy, Mutah University, Al-Karak, 61710, Jordan.*

Summary

Bio-based 5-hydroxymethylfurfural (HMF) serves as an important platform for several chemicals, among which 2,5-furan dicarboxylic acid (FDCA) has attracted considerable interest as a monomer for the production of polyethylene furanoate (PEF), a potential alternative for fossil-based polyethylene terephthalate (PET). This study is based on the HMF oxidizing activity shown by *Mycobacterium* sp. MS 1601 cells and investigation of the enzyme catalysing the oxidation. The *Mycobacterium* whole cells oxidized the HMF to FDCA (60% yield) and hydroxymethyl furan carboxylic acid (HMFCA). A gene encoding a novel bacterial aryl alcohol oxidase, hereinafter *Mycsp*AAO, was identified in the genome and was cloned and expressed in *Escherichia coli* BI21 (DE3). The purified *Mycsp*AAO displayed activity against several alcohols and aldehydes; 3,5 dimethoxy benzyl alcohol (veratryl alcohol) was the best substrate among those tested followed by HMF. 5-Hydroxymethylfurfural was converted to 5-formyl-2-furoic acid (FFCA) via diformyl furan (DFF) with optimal activity at pH 8 and 30–40°C. FDCA formation was observed during long reaction time with low HMF concentration. Mutagenesis of several amino acids shaping the active site and evaluation of the variants showed Y444F to have around 3-fold higher k_{cat}/K_m and ~1.7-fold lower K_m with HMF.

Received 10 April, 2021; revised 6 March, 2022; accepted 8 March, 2022.

For correspondence. *E-mail rajni.hatti-kaul@biotek.lu.se; Tel. (+46) 46 222 4840; Fax (+46) 46 222 4713.

Present address: †Department of Chemical, Biological and Environmental Engineering, Universitat Autonoma Barcelona, Bellaterra, Spain.

Microbial Biotechnology (2022) **15**(8), 2176–2190
doi:10.1111/1751-7915.14052

Funding information

Swedish Foundation for Strategic Environmental Research (Mistra) (grant no. 2016/1489); Swedish Research Council FORMAS (grant no. 942-2016-33).

Introduction

Oxidation of 5-hydroxymethylfurfural (HMF), a dehydration product of C6 sugars, has been a reaction of interest to provide oxidized derivatives, especially 2,5-furan dicarboxylic acid (FDCA) for use as building block for the polyester polyethylene furanoate (PEF), a biobased alternative to the widely used polyethylene terephthalate (PET). Replacement of one tonne of PET with PEF is expected to reduce the greenhouse gas emission by 30–50% (Davidson *et al*., 2021). Polyethylene furanoate has also the advantage of possessing better barrier, thermal and mechanical features (Sousa *et al*., 2015, 2016). Both HMF and FDCA are identified by the US Department of Energy to be among the important biobased platform chemicals with no negative effect on environment and human health (Werpy *et al*., 2004; Bozell and Petersen, 2010; Sousa *et al*., 2015; Chen *et al*., 2016; Troiano *et al*., 2020). Besides replacing terephthalic acid, FDCA can also replace adipic acid (Sousa *et al*., 2015, 2016; Zhang and Deng, 2015; Yuan *et al*., 2018, 2020) and can serve as a platform to produce other important chemicals such as succinic acid, 2,5-diformyl furan (DFF), 2,5-bis(hydroxymethyl)furan (BHMF) and 2,5-(bishydroxymethyl) tetrahydrofuran (Werpy *et al*., 2004; Zhang *et al*., 2015).

2,5-Furan dicarboxylic acid production from HMF involves three oxidation steps and can proceed via two different pathways (Scheme 1). In the first pathway (A), the alcohol group of HMF **(1)** is oxidized to an aldehyde giving 2,5-diformylfuran (DFF) **(2*)**, followed by further oxidation of the two aldehyde groups in DFF to FDCA **(5)** through 5-formyl-2-furoic acid (FFCA) **(4)**, while the second pathway (B) involves oxidation of the aldehyde group of HMF to 5-hydroxymethyl-2-furoic acid (HMFCA) **(3)**, followed by further oxidation of the hydroxyl group of

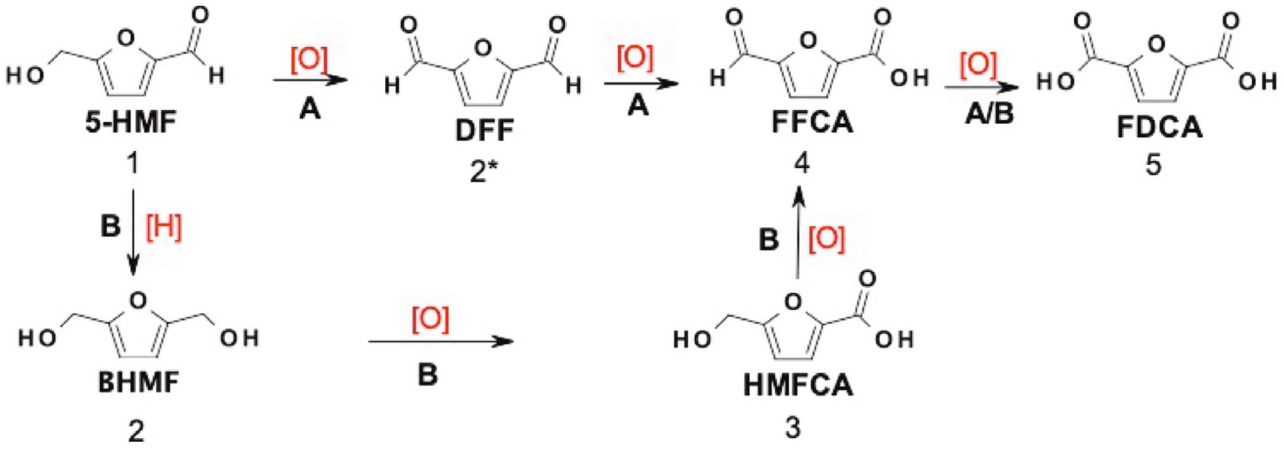

Scheme 1. Biocatalytic reaction pathways (A and B) for production of FDCA from HMF by three-step oxidation [O]. The pathway B involves a reduction [H] step prior to oxidation.

HMFCA to FDCA via FFCA (Dijkman, 2015; Dijkman *et al.*, 2015; Troiano *et al.*, 2020; Yuan *et al.*, 2020). Several reports on the oxidation of HMF via chemocatalysis, (photo-)electrochemical catalysis or biocatalysis are available (Ribeiro and Schuchardt, 2003; Chadderdon *et al.*, 2014; Zhang and Deng, 2015; Carro *et al.*, 2018a; Sajid *et al.*, 2018; Sayed *et al.*, 2020; Troiano *et al.*, 2020; Yuan *et al.*, 2020; Kawde *et al.*, 2021). Biocatalytic oxidation of HMF and other aliphatic and aromatic alcohols, diols and polyols using enzymes or microbial cells offers a facile and selective route of reaction under mild conditions. Many microorganisms including bacteria and fungi have shown the ability to metabolize HMF to different products including FDCA (Yuan *et al.*, 2020). In some microorganisms, the HMF oxidizing activity has been attributed to HMF oxidase (HMFO), which is expected to form FDCA as the final product (Dijkman, 2015; Troiano *et al.*, 2020; Vinambres *et al.*, 2020). Besides HMFO, other reports describe the use of a cascade of enzymes for achieving oxidation of HMF to FDCA. For example, a cascade of galactose oxidase M3-5 variant, that oxidizes HMF to DFF, and *Escherichia coli* periplasmic aldehyde oxidase ABC, oxidizing DFF to FFCA, and consequently to FDCA has been reported (McKenna *et al.*, 2017). This pathway was further developed by including horseradish peroxidase and lipase B from *Candida antarctica* (McKenna *et al.*, 2015, 2017). The potential drawbacks of an enzyme cascade system could be the differences in the optimum reaction conditions for the enzymes involved and the cost of enzymes production (Troiano *et al.*, 2020).

Glucose–methanol–choline oxidoreductase (GMC) family includes flavoprotein oxidoreductases that are classified into several subfamilies acting on a wide range of substrates from short alcohols such as methanol and choline to more complex substrates such as glucose, aromatic alcohols, fatty alcohols among others (Sützl *et al.*, 2019; Aleksenko *et al.*, 2020; Savino and Fraaije, 2021). According to the Pfam database, GMC oxidoreductases include two domains; the first is Pfam00732 with a typical GxGxxG/A motif, an indicator for the Rossman fold, and responsible for binding the adenosine diphosphate (ADP) moiety of the flavin adenine dinucleotide (FAD) prosthetic group, while the second is the less conserved C-terminal domain, which usually contributes to the substrate specificity of the enzyme. A characteristic of these oxidoreductases is a conserved histidine in the active site that initiates the oxidation via proton subtraction from the substrate and assists in FAD re-oxidation by the molecular oxygen. Among the subfamilies of GMC oxidoreductases are aryl alcohol oxidases (AAOs) that have been reported to oxidize HMF (Serrano *et al.*, 2020; Lappe *et al.*, 2021). Aryl-alcohol oxidases (AAOs; EC 1.1.3.7) catalyse the oxidative dehydrogenation of primary alcohols from aliphatic unsaturated or aromatic alcohols to aldehydes using oxygen as a final electron acceptor resulting in production of hydrogen peroxide (H_2O_2) (Urlacher and Koschorreck, 2021). Aryl alcohol oxidases have also been classified in the CAZy (the carbohydrate-active enzymes) database into subfamily AA3_2, where AA3 refers to Auxiliary Activity (AA) superfamily that comprises four subfamilies with different GMC oxidoreductases (Sützl *et al.*, 2018). These enzymes are known to play an important role in biomass degradation by way of supplying hydrogen peroxide to the ligninolytic peroxidases.

Mycobacterium sp. MS1601 is a promising source of enzymes for oxidation reactions, which is evident from the abundance of gene sequences encoding oxidases and dehydrogenases in its genome (Sayed *et al.*, 2017a). The organism has shown unique activity for selective oxidation of branched polyols such as

trimethylolpropane (TMP) to 2,2-bis(hydroxymethyl) butyric acid (BHMB) with high selectivity and yield (Sayed *et al.*, 2016, 2017a) and was also recently shown to oxidize 1,6-hexanediol to 6-hydroxyhexanoic acid and adipic acid (Pyo *et al.*, 2020).

This report presents a study demonstrating the ability of *Mycobacterium* sp. MS1601 to oxidize HMF to FDCA and other oxidized intermediates, identification of a novel aryl alcohol oxidase (*Mycsp*AAO) in the bacteria that efficiently catalyses oxidation of HMF, heterologous production of the enzyme in *Escherichia coli* and determination of its substrate scope. Furthermore, through sequence and structure analysis based on homology modelling, an important mutation was generated that resulted in improved HMF oxidation and also revealed FDCA production.

Results

Oxidation of HMF using Mycobacterium *sp. MS 1601 cells*

Mycobacterium sp. MS1601 cells grown in the medium with different carbon sources including glycerol, glucose and sorbitol, respectively, were used for reaction with 5 mg ml^{-1} (39.6 mM) HMF for 120 h. Complete consumption of HMF was observed in all cases, but only the cells activated with glycerol showed the ability to produce FDCA with around 60% yield and selectivity and the remaining 40% was represented by HMFCA (Fig. 1A). Formation of FFCA and BHMF was observed in the initial stage of the reaction and reached a maximum yield of 30.8% and 16%, respectively, before being converted to FDCA and HMFCA, respectively (Fig. 1A). Meanwhile, the cells grown with glucose or sorbitol as carbon source, led to the accumulation of BHMF and HMFCA as products (Fig. 1B and C). BHMF reached a yield of 82% and 77.3% after 12 h of the reaction with the *Mycobacterium* cells activated with glucose and sorbitol, respectively, and was thereafter gradually converted to give 61.6% and 65.8% of HMFCA in the two cases at 120 h of the reaction. The reaction profiles revealed that the enzyme(s) catalysing the reduction of HMF to BHMF were activated more by glucose.

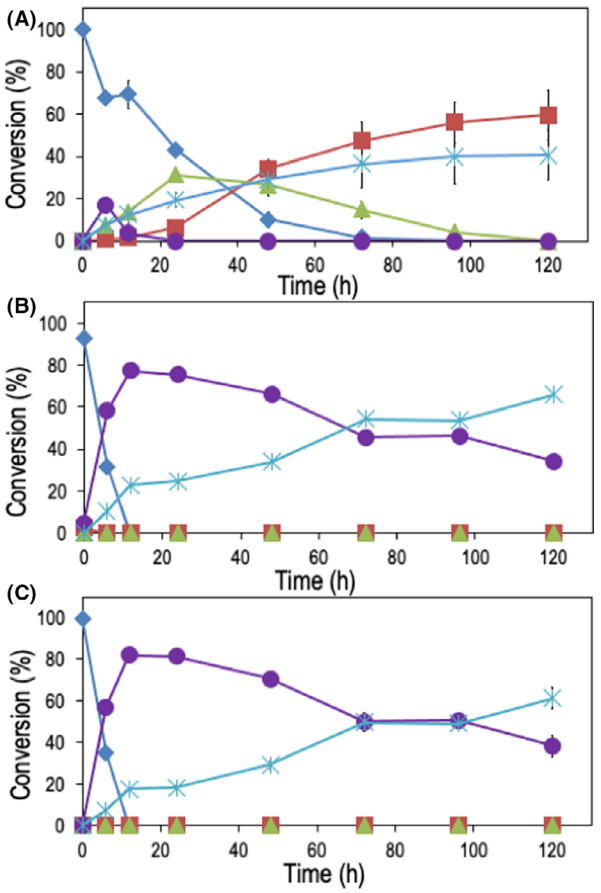

Fig. 1. Oxidation of HMF (5 g l^{-1}) (♦) to FDCA (■), HMFCA (v), FFCA (▲) and BHMF (●) using resting cells of Mycobacterium sp. MS1601, which were grown and activated in 5 g l^{-1} of different carbon sources: (A) glycerol, (B) sorbitol, and (C) glucose, respectively. Experimental details are described in the text. Experiments were carried out in duplicates and the data shown represents the mean and standard deviation from the replicates.

Mycsp*AAO identification and sequence analysis*

To identify the putative HMF oxidizing enzymes in the *Mycobacterium* sp. M1601, BLAST search focused only on the genome using *Metsp*HMFO sequence, the HMFO from *Methylovorus* sp., as a query sequence, was performed (Dijkman and Fraaije, 2014). The search resulted in three candidate sequences, namely A0A1P8X5Y5, A0A1P8XFW1 and A0A1P8XIE5 that showed putative oxidase features. The three sequences were preliminary annotated as GMC oxidoreductases and showed reasonable sequence identities of 33%, 29% and 25%, respectively, to *Metsp*HMFO. Further analysis of the A0A1P8X5Y5 sequence using HAMMER server and Pfam databases indicated the presence of the two GMC Pfam domains i.e., GMC_oxred_N (PF00732) and GMC_oxred_C (PF05199). BLAST search using A0A1P8X5Y5 sequence to the Uniprot database retrieved 250 hits that have been annotated as choline dehydrogenase, alcohol dehydrogenase and GMC oxidoreductases among others. The highest sequence identity retrieved was 78.4% while the lowest was 43.5% (Fig. S1A–C), however none of these 250 hits have been experimentally characterized up-to-date. Alignment with the characterized CAZY AA3 proteins showed A0A1P8X5Y5 sequence to cluster with AA3_2 subfamily (Fig. S1B). Alignment with the fungal GMC oxidoreductases further revealed certain conserved residues

including the catalytic histidine (Fig. S1C and D). To this end, we decided to codon optimize and synthesize the DNA sequence of A0A1P8X5Y5 (Fig. S2), henceforth called as *Mycsp*AAO, for expression in *E. coli*.

Phylogenetic analysis of the A0A1P8X5Y5 sequence against the HMFOs and AAOs that have been experimentally characterized so far, showed the relatedness of the bacterial HMFOs to each other, while that of the fungal AAOs to each other (Fig. 2). *Mycsp*AAO has been located in-between these two subfamilies since it is a bacterial AAO. Since there is no published sequence of a characterized bacterial AAO up-to-date, they were not included in this phylogenetic analysis. The multiple sequence alignment of *Mycsp*AAO to the three characterized HMFOs showed specific variations in the sequence motifs that have been recently described (Vinambres *et al*., 2020). These variations are as follows: the ADP-binding domain – GAG instead of GGG conserved motif, in the active site region – VYYH instead of WVWH, in the PS000623 motif – PRGH instead of EQGR and in the PS000624 motif – GGA instead of AGA (Fig. S3).

Overexpression of MycspAAO *and its mutants in* E. coli

Escherichia coli BL21 (DE3) transformed with *Mycsp*AAO gene was grown in NYAT and Terrific Broth (TB) medium, and the gene expression after induction was tested at 15, 20 and 30°C, respectively. Determination of HMF oxidizing activity in the clarified cell lysate after cell disruption showed conversion of HMF (4 mM) to be higher with the recombinant cells from the TB medium, corresponding to 97%, 88% and 90% for the cells with gene expression at 15, 20 and 30°C, respectively (Fig. S4A). In the NYAT medium, only the cells induced at 15°C provided an active cell lysate giving HMF conversion of 84%, while the lysates from the cultures at 20 and 30°C gave HMF conversion of only 14 and 0.5%, respectively (Fig. S4B). *Escherichia coli* cells carrying the plasmid without the *Mycsp*AAO gene showed no conversion of HMF. Hence, for further experiments, cultivation in TB and gene expression at 15°C were chosen for *Mycsp*AAO production in *E. coli* BL21 (DE3). The enzyme was purified from the cell lysate by metal ion affinity chromatography and was obtained as a protein with an estimated molecular weight of 54 kDa by SDS-PAGE. The purified yellow-coloured *Mycsp*AAO, obtained at a concentration of about 1 mg ml^{-1} was used for further experiments. The enzyme was confirmed as a FAD dependent oxidase through its thermal denaturation and spectrophotometric measurement of the released FAD at 450 nm (not shown).

Mycsp*AAO substrate spectrum and optimum conditions for activity*

Preliminary screening of *Mycsp*AAO activity was performed against a range of compounds using a common assay coupled with horseradish peroxidase catalysed determination of H_2O_2 released (Fig. 3A). *Mycsp*AAO exhibited higher specific activity, 4.95, 4.09, 3.79, 3.63 and 3.16 U mg^{-1} with 3,4-DMBA, HMF, DFF, BHMF and MBA, respectively, as substrates. The specific activity values were 1.2, 0.94, 0.66, 0.23 and 0.12 U mg^{-1} with 4HBA, furfural, BA, FFCA and HMFCA, respectively. While the activity against the aliphatic alcohol, *n*-propanol was in the same range (0.13 U mg^{-1}), activity against choline, pyridoxine, glycerol and glucose was extremely low (Fig. 3C). No colour was observed in the control reaction mixtures without *Mycsp*AAO (Fig. S5).

Optimum temperature and pH for oxidation of HMF by *Mycsp*AAO were then determined by chromatographic analysis of the substrate and products. The *Mycsp*AAO activity showed a rather broad pH profile between pH 5–9, with the highest activity at pH 8 giving 93% HMF conversion in 2 h (Fig. 3B). Reactions performed with 4 mM HMF at pH 8 showed the highest substrate conversion (98%) at 40°C followed by 94% at 30°C, while the enzyme activity was drastically decreased at 60°C and above (Fig. 3C).

Subsequently, *Mycsp*AAO was used for oxidation of 4 g l^{-1} HMF (31.7 mM) at pH 8 and 30°C for a longer time period. The reaction profile in Fig. 4 shows DFF to

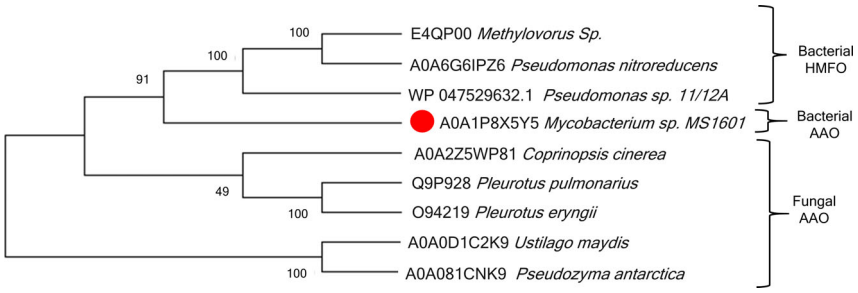

Fig. 2. Phylogenetic analysis of the A0A1P8X5Y5 sequence (*Mycsp*AAO) in the genome of Mycobacterium sp. MS1601 with bacterial HMFO and fungal AAO sequences described with enzymatic activities in literature. Analysis is done using Mega X software.

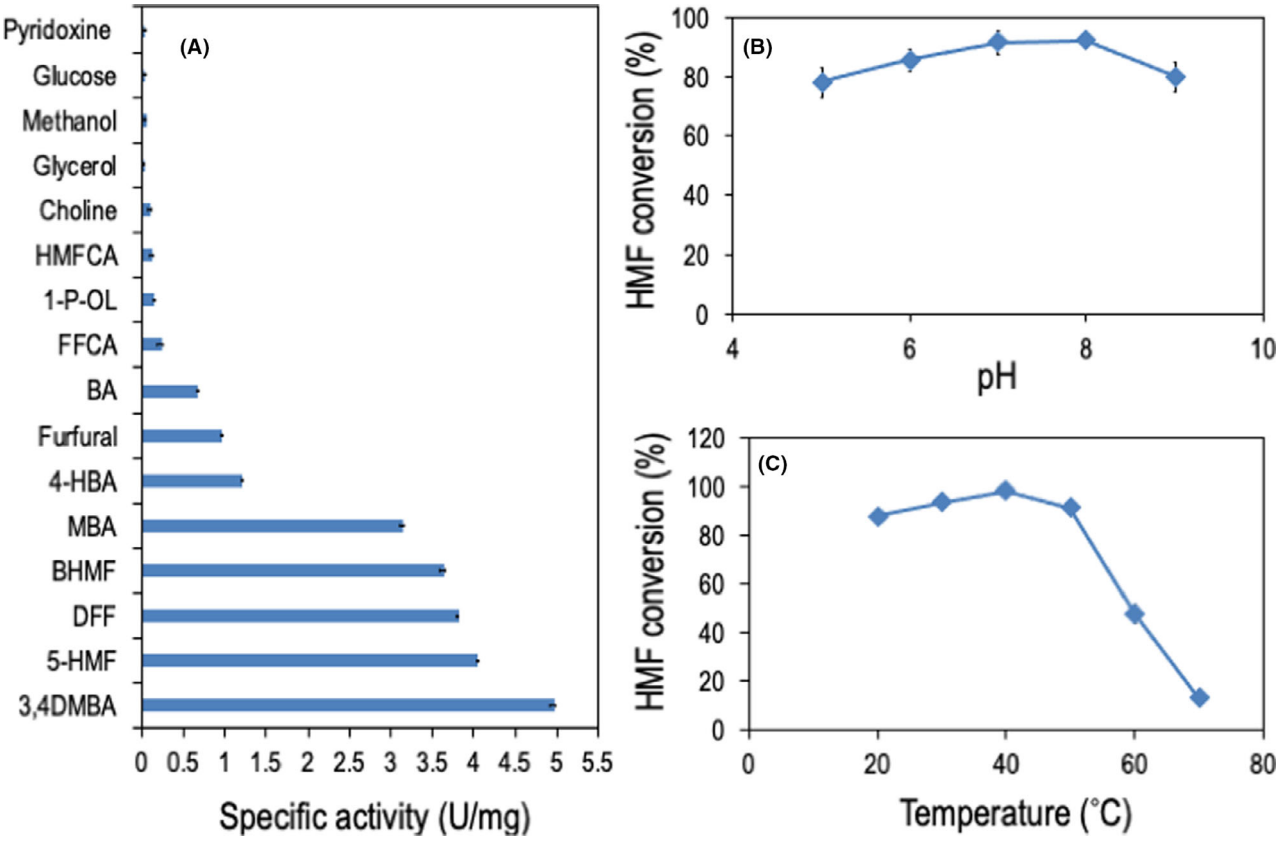

Fig. 3. Specific activity of *Mycsp*AAO-WT against different aliphatic, aromatic alcohols, and putative substrates for the GMC oxidoreductase enzymes at pH 8 and 30°C (A). Effect of (B) pH and (C) reaction temperature on the conversion (%) of HMF (4 mM) using purified *Mycsp*AAO-WT (40 μg ml^{-1}) after 2 h reaction. The reaction at different temperatures was performed at pH 8, while the effect of pH was studied at 30°C. All experiments in (A) were carried out in 4 replicates, and experiments for (B) and (C) were done in duplicates. The data in all the figures represent the mean and standard deviation from the replicates.

be the first oxidation product, which was totally converted to FFCA with 100% yield and selectivity. No FDCA was observed in the reaction.

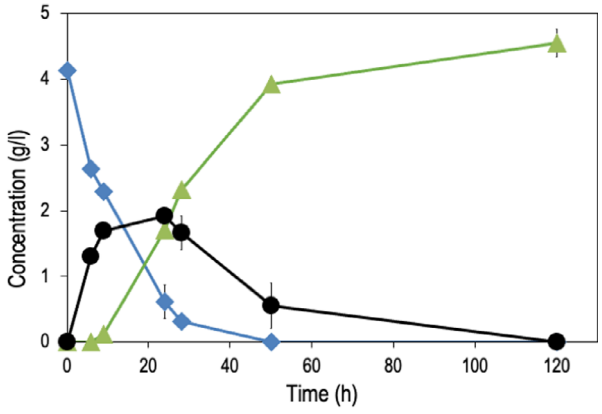

Fig. 4. Profiles of HMF (♦) oxidation to DFF (●) and FFCA (▲) during the reaction of 31.7 mM HMF (4 g l^{-1}) with the purified *Mycsp*AAO-WT (200 μg ml^{-1}) at 30°C and pH 8. The experiment was done in duplicate and the data shown represents the mean and standard deviation from the replicates.

Homology modelling and mutagenesis of Mycsp*AAO*

The three-dimensional structure of *Mycsp*AAO was predicted through homology modelling, and the final model obtained was assessed using the Swiss model assessment server (Fig. S6). The Ramachandran plot showed that 95.2% of the residues are located in the allowed region, and zero outliers were recorded. The normalized QMEAN Score for the model was < 1, which indicates acceptable model quality (Fig. S7).

The obtained *Mycsp*AAO 3D model (Fig. S6) showed the basic features of GMC oxidoreductases, including the Rossman fold that holds the FAD cofactor and the C-terminal domain. *Mycsp*AAO does not have the conserved His/His residues, instead a His/Asn was observed. Moreover, the enzyme binds non-covalently to the FAD cofactor due to the missing conserved His in the position 91, which is replaced by Ile. The model has been compared with the PDB 3FIM (fungal AAO of *Pleurotus eryngii*) (Fig. 5). The comparison showed the presence of the characteristic loop located in front of the

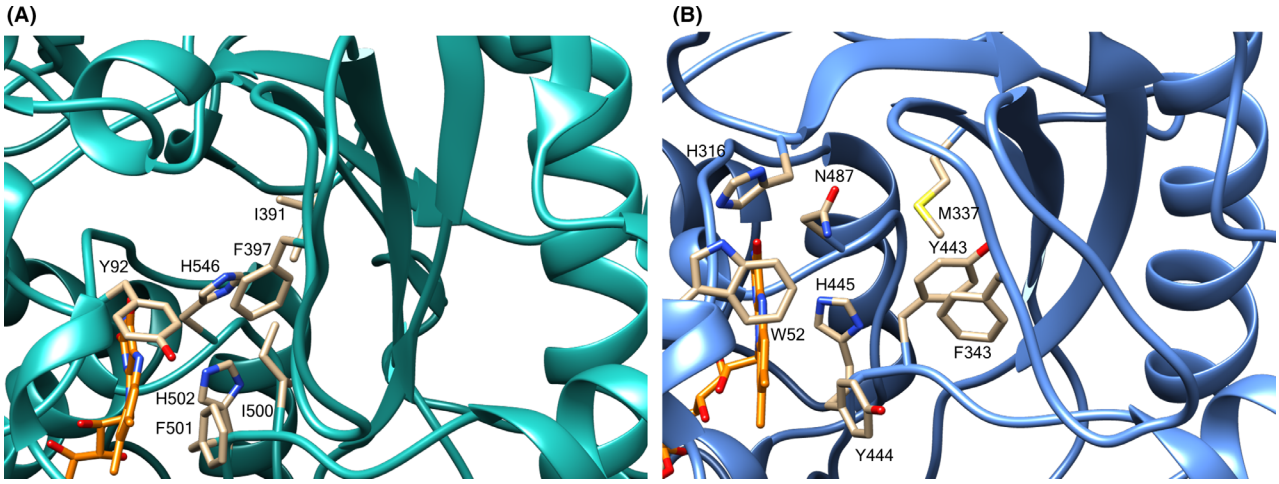

Fig. 5. Comparison of the active site of an aryl alcohol oxidase, PDB 3FIM (A) to the model of *Mycsp*AAO (B) in the present study. The loop covering the FAD controlling the substrate entrance and product release is shown in the panel. The comparable residues are as follows 3FIM: I500, F501, H502, H546, I391, F397 and the counterpart residues in *Mycsp*AAO are Y443, Y444, H445, N487, M337 and F343. The aromatic residues in *Mycsp*AAO W52, H316, F343, Y444 and Y443 are probably contributing to the substrate specificity and oxygen activation by the FAD cofactor.

active site that has been described to control the access of the substrates to the active site (Fig. 5B) (Carro *et al.*, 2018b).

Upon investigation of the active site of *Mycsp*AAO based on the model structure generated in this study, we noticed the narrow active site was due to the presence of two tyrosine residues Y443 and Y444 in the substrate-binding site facing the FAD molecule (Fig. S8). These two residues were thus listed for site directed mutagenesis. The residues that were probably interacting and to the substrate binding were as follows: Y443, Y444, L298, M337, V360, A358, A93 and V95. Based on these observations, 11 mutations were proposed (Table S1) and were carried out using the primers designed for site-directed mutagenesis of the different amino acid residues.

Out of the eleven mutations planned, expression of only seven enzyme variants was successfully obtained. Screening of the activity of the variants against 2.5 mM HMF using clarified cell lysates (obtained from cell suspensions with similar OD_{600}) and HPLC analysis of the reaction sample after 48 h, showed huge activity reduction for most of the variants i.e., Y444A, L298S, V95A, M377F and A358R, while L298A variant showed slightly lower activity than the wild-type *Mycsp*AAO (Fig. 6). Y444F was the only variant with higher activity compared with *Mycsp*AAO-WT.

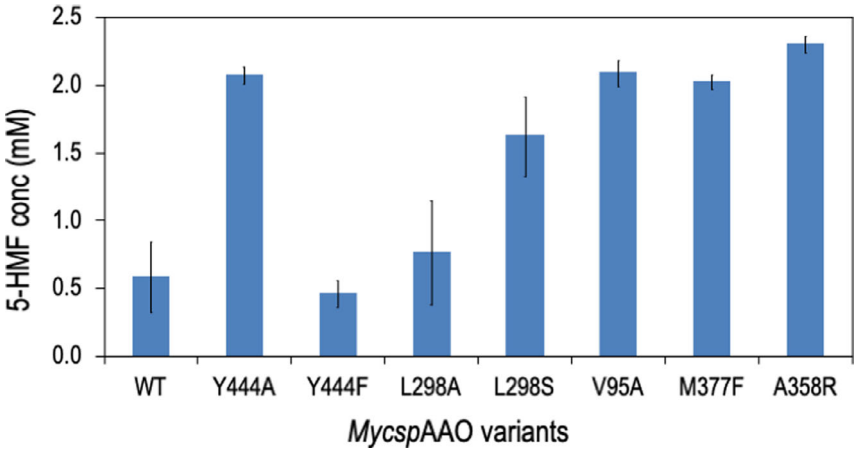

Fig. 6. Residual HMF concentration after 48 h during activity screening of the clarified cell lysates of *E. coli* expressing *Mycsp*AAO-WT and the mutant enzymes against 2.5 mM HMF at 30°C and pH 8. The higher bars indicate lower activity. All reactions were carried out in duplicates and results in the figure represent the mean and standard deviation from the replicates.

Kinetic parameters and FDCA production

Y444F and L298A variants as well as the wild-type *Mycsp* AAO were then produced in one-litre medium and purified. The purity of the proteins was checked using SDS-PAGE (Fig. S9), and concentrations were determined using BCA reagent based on BSA standard (Table S3). Figure S10 shows the initial reaction rate (V) for HMF oxidation at different concentrations by the wild-type (WT), Y444F and L289A enzymes during 3 h reaction time. Y444F showed a significant increase in the reaction rate up to 10 mM HMF, above which there was a drastic decrease in activity and the reaction rate remained constant up to 60 mM HMF (Fig. S10). For the WT and L289A enzymes, the reaction rate decreased above 4 mM HMF, and further decrease was observed above 40 mM HMF. At 10 mM HMF, the initial activity of Y444F was around 10 times higher than the other *Mycsp*AAO variants.

Determination of the steady-state kinetic parameters of the enzyme variants revealed *Mycsp*AAO-Y444F to have around two-fold higher k_{cat} and V_{max}, 1.7-fold lower K_m and about 3-fold higher k_{cat}/K_m, compared with *Mycsp*AAO-WT (Table 1). On the other hand, the L298A variant showed almost same k_{cat} and V_{max}, and K_m with slight difference compared with the wild-type enzyme (Table 1).

*Mycsp*AAO-WT and -Y444F (200 μg ml^{-1} total protein) were further used for oxidation of 10 mM HMF (lower concentration than that in Fig. 3). Both enzymes oxidized HMF completely within 6 h mainly to DFF; the formation of DFF is seen already at 0 h reaction (immediately after addition of the enzymes) and is higher with the Y444F variant (Fig. 7A). Diformyl furan is subsequently converted to FFCA. Further oxidation of FFCA to FDCA by both WT and the mutant enzyme was observed after 96 h of reaction (Fig 7A). The oxidation rate of HMF to DFF as well as DFF to FFCA was higher with *Mycsp*AAO-Y444F compared with the wild-type enzyme, confirming the findings from the colorimetric assay as well as the kinetic parameters above (Fig. 7 and Table 1).

Discussion

The genome sequence of *Mycobacterium* sp. MS1601 shows the presence of many gene sequences that are annotated as oxidative enzymes (296 dehydrogenases; 168 oxidoreductases and 53 oxidases) (Sayed *et al.*, 2017b). The organism has so far been used as an efficient biocatalyst for the highly selective oxidation of polyhydric alcohols (Sayed *et al.*, 2016, 2017b), and in this study for the oxidation of HMF. Interestingly, oxidation of HMF by *Mycobacterium* sp. MS1601 seems to follow different routes depending on the carbon source used for growing the cells. While the cells grown on glycerol, oxidized HMF to FDCA via FFCA (pathway A in Scheme 1) (Fig. 1A), a typical pathway used by HMFO from *Methylovorus* sp. MP688 (Dijkman and Fraaije, 2014), oxidation by the cells grown on glucose or sorbitol followed an alternative route in Scheme 1 yielding BHMF and HMFCA that was not oxidized further (Fig. 1B and C). In the latter case, the aldehyde group of HMF is either oxidized directly to HMFCA or after first being reduced to BHMF. Activation of the enzyme(s) responsible for FDCA production with glycerol was in agreement with the previous report involving selective oxidation of trimethylolpropanol (TMP) to its corresponding carboxylic acid by *Mycobacterium* sp. MS1601 (Sayed *et al.*, 2017b).

Based on the similarity of the HMF oxidation profile by the glycerol-activated cells to that by *Metsp*HMFO, the sequence of the *Methylovorus* sp. enzyme was used for probing the *Mycobacterium* sp. MS1601 genome for homologous enzymes. The putative gene sequence with > 30% identity with *Metsp*HMFO was chosen for this study. Since the identity to *Metsp*HMFO was low, further sequence analysis was done for the chosen gene from *Mycobacterium* sp. MS1601 using Pfams and Uniport databases, confirming that the chosen sequence encodes an enzyme belonging to GMC family, to which *Metsp*HMFO also belongs (Dijkman and Fraaije, 2014). However, the first 250 hits from Uniport analysis with high identity were for other GMC members that are not yet experimentally characterized. This observation confirmed the novelty of the chosen protein from *Mycobacterium* sp. MS1601. The codon-optimized gene of the above-mentioned gene from *Mycobacterium* sp. MS1601was expressed in a soluble form in *E. coli* BL21 (DE3) at 15°C. The purified *Mycsp*AAO was shown to be a wide spectrum GMC oxidase enzyme that utilizes oxygen as the final electron receptor and prefers compounds with an aromatic ring as 3,4-DMBA>HMF>DFF>BHMF>MBA>4-HBA> furfural>BA compared with aliphatic substrates (Fig. 3A). The high specific activity of *Mycsp*AAO against 3,4-DMBA, MBA and BA is in agreement with the activity of bacterial aryl alcohol oxidase from *Sphingobacterium* sp. ATM (Tamboli *et al.*, 2011). Our findings indicate that the new GMC member from *Mycobacterium* sp. MS1601 belongs to the subfamily of aryl alcohol oxidases, also displaying high activity against HMF and its derivatives including DFF and BHMF (Fig. 3A). Reactions with DFF

Table 1. Steady-state kinetic parameters of the activities of *Mycsp*HMFO and its variants against HMF at 30°C and pH 8. The experiments for the kinetic parameters were done in duplicates.

	V_{max} (mM min^{-1})	K_m (mM)	k_{cat} (s^{-1})	k_{cat}/K_m (mM^{-1} s^{-1})
WT	0.04 ± 0.004	3.3 ± 0.3	384 ± 33.5	115 ± 1.6
L289A	0.038 ± 0.002	3.1 ± 0.17	350 ± 17.8	113 ± 0.3
Y444F	0.072 ± 0.0002	1.9 ± 0.005	652 ± 1.7	342 ± 0.0

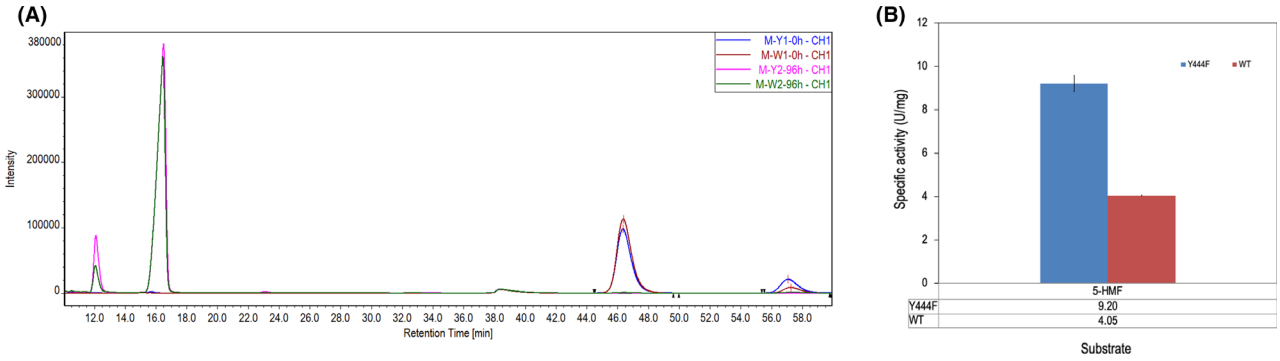

Fig. 7. (A) HPLC profiles of the reactions at 0 and 96 h during oxidation of 10 mM 5-HMF using the purified *Mycsp*AAO-WT (W) and Y444F (Y) (total protein concentration of 300 μg ml^{-1}), revealing FDCA, FFCA, 5-HMF and DFF at retention times of 12, 15.6, 46.3 and 57.5 min, respectively. Peaks for HMF and DFF (red colour for WT and blue for Y444F) are seen only in the 0 h sample, and FFCA and FDCA peaks (green colour for WT and pink colour for Y444F) are observed in the 96 h reaction sample. The reactions were performed in duplicates. (B) Specific activities of *Mycsp*AAO-WT and -Y444F (total protein concentration of 80 μg ml^{-1}) against 5 mM HMF using the colorimetric assay after 30 min reaction. The data represents the mean and standard deviation of four replicates.

and furfural as substrates suggest that the enzyme is active also on the aldehyde groups; the oxidation of DFF and BHMF resulted in the formation of FFCA. Aryl alcohol oxidases in rare cases have been shown to catalyse the oxidation of aromatic aldehyde substrates to the corresponding acids (Urlacher and Koschorreck, 2021), which is proposed to proceed via the *gem*-diols formed by aldehyde hydration and hence following the mechanism similar to alcohol oxidation (Ferreira *et al*., 2010). *Mycsp*AAO displayed very low activity against FFCA and HMFCA as observed even for other AAOs (Carro *et al*., 2015; Serrano *et al*., 2019; Viña-Gonzalez *et al*., 2020; Lappe *et al*., 2021), which may be due to interference by the carboxylic group on the binding of the substrate to the enzyme active site.

More insights were gained from comparison of *Mycsp*AAO to the closest fungal aryl alcohol oxidase PDB 3FIM. A characteristic loop covering the active site has been described in the case of PDB 3FIM, and interestingly a similar loop has been identified in the *Mycsp*AAO model. Most importantly, the previously reported F397 in 3FIM has an equivalent residue F343 in *Mycsp*AAO (Fig. 5). This phenylalanine residue is proposed to attach to the substrates and to be involved in a significant loop displacement necessary to place the substrate inside the active site (Carro *et al*., 2018b; Serrano *et al*., 2020). Moreover, the analysis of *Mycsp*AAO 3D model showed a narrow active site due to the presence of two tyrosine residues (Y443 and Y444) located very close to the catalytic H445. These two tyrosine residues may be expected to cause interference for the bulkier substrates to be accepted by the enzyme.

*Mycsp*AAO-Y444F exhibits favourable kinetic parameters against HMF, 4HBA, and furfural compared with the wild-type enzyme (Table 1 and Fig. S11). With HMF, the improved activity of the enzyme variant was ascribed to the significantly higher k_{cat}/K_m and lower K_m values (Table 1). The higher activity of *Mycsp*AAO-Y444F can be further related to the observations recorded for the fungal AAO (PDB 3FIM). F444 in the enzyme variant is exactly equivalent to the F501 in the fungal AAO (3FIM) structures, which is proposed to be a major player in the substrate activity and specificity. This phenylalanine has also been described to control the access of molecular oxygen to the FAD molecule in the active site (Hernandez-Ortega *et al*., 2011; Ferreira *et al*., 2015; Carro *et al*., 2018b) Hence, *Mycsp*AAO-Y444F denotes a back-to-ancestral mutation since phenylalanine residue is conserved in many GMC oxidoreductases and specifically in most of the AAOs that have been characterized up to date (Chakraborty *et al*., 2014; Galperin *et al*., 2016; Jankowski *et al*., 2020).

Both *Mycsp*AAO-WT and *Mycsp*AAO-Y444F variants, when tested against a lower concentration of HMF (10 mM in contrast to 31.7 mM) revealed the formation of FDCA over a long incubation time, the Y444F variant giving the higher activity (Fig. 7). These observations are in agreement with that reported previously for HMFOs and AAOs (Cavener, 1992; Dijkman *et al*., 2014; Serrano *et al*., 2019; Vinambres *et al*., 2020). Very recently, Sánchez-Ruiz *et al*. (2021) reported that FFCA, especially at higher concentration (over 15 mM) has an irreversible inhibition against HMFOs (Sánchez-Ruiz *et al*., 2021), which could explain FDCA formation from 10 mM HMF (Fig. 7), and not during the oxidation of 31.7 mM HMF with *Mycsp*AAO-WT (Fig. 3). This finding was further confirmed from screening *Mycsp* AAO-WT, -Y444F and L298A variants against concentrations of HMF (Fig. S10), that showed that increasing the concentration of HMF over 10 mM reduced the initial activity of all the variants although the Y444F variant showed a significantly higher activity.

In summary, this report indicates that *Mycobacterium* sp. MS1601 is an interesting source of enzymes for oxidation of HMF. While the whole cells showed the formation of products with different levels of oxidation including FDCA, the analysis of the selected gene sequence from the genome of *Mycobacterium* sp. MS1601 indicates that the HMF oxidizing enzyme represents a novel bacterial AAO that oxidizes HMF preferably to FFCA but even to FDCA at lower substrate concentration and longer reaction time. The site-directed mutagenesis studies on *Mycsp*AAO indicated that the Y444 in the enzyme's active site could be replaced by the conserved phenylalanine (F) for improved enzymatic activity. Further improvement through introducing additional rational mutations in *Mycsp*AAO are required to increase the capacity of *Mycsp*AAO to oxidize HMF completely to FDCA in a shorter reaction time and higher substrate concentration. On the other hand, being host to several oxidative enzymes, it is more likely that *Mycobacterium* sp. MS1601 cells utilize an aldehyde dehydrogenase/oxidase activity for oxidation of FFCA *in vivo*.

Experimental procedures

Materials

Mycobacterium sp. MS1601 (previously, *Corynebacterium* sp. ATCC 21245) was obtained from American Type Culture Collection (ATCC, USA). Ampicillin, kanamycin, bovine serum albumin, bicinchoninic acid (BCA), 5-hydroxymethyl furfural (HMF), 2-formyl-5-furan carboxylic acid (FFCA), 2,5-diformyl furan (FFA), 2,5 furan dicarboxylic acid (FDCA), sorbitol and glucose were purchased from Sigma-Aldrich. Yeast extract, glycerol, sodium acetate, sodium dihydrogen phosphate and disodium hydrogen phosphate were from Merck. All chemicals were of analytical grade. *Escherichia coli* (DH5α) and One Shot™ Top10 Comp cells for cloning, *E. coli* BL21 (DE3) for protein expression, and the pET-22b(+) and pRSF-Duet vectors were acquired from Novagen (Madison, WI), while the restriction enzymes, EcoRI, XhoI, T4 DNA ligase and QuickChange™ site-directed mutagenesis kits were from Thermo Fisher Scientific (Waltham, MA, USA). Isopropyl β-D-1-thiogalactopyranoside (IPTG) was purchased from Saveen & Werner AB (Limhamn, Sweden).

Cultivation of Mycobacterium *sp. MS1601 for oxidation of HMF*

The stock culture of *Mycobacterium* sp. MS1601 was prepared by aseptically transferring the lyophilized culture to 25 ml of sterile nutrient broth containing per litre: 5 g peptone and 3 g beef extract (pH 6.8) in a 250 ml Erlenmeyer flask. The flask was incubated in an orbital-shaking incubator (Ecotron, Infors HT, UK) at 31°C and 300 rpm for 48 h. The resulting culture was mixed with sterile 20% (v/v) glycerol and then stored at −20°C.

For activation of the *Mycobacterium* sp. MS1601 cells for HMF oxidation, 200 µl of the glycerol stock culture was added to 50 ml sterile activation medium containing per litre: 5 g glycerol, sorbitol or glucose as carbon source, 2 g sodium acetate and 10 g yeast extract in 250 ml Erlenmeyer flask. The culture was incubated as above for 48 h. Four millilitres of the culture broth were withdrawn, centrifuged and washed with 100 mM phosphate buffer pH 8, which was also used as reaction buffer. The cells were then suspended in 1 ml reaction buffer supplemented with 5 mg ml^{-1} (39.6 mM) HMF in 4 ml vials. The vials were incubated in a thermomixer (MKR 13, HLC Biotech, Germany) at 30°C and 500 rpm. Samples of 50 µl were collected at regular time intervals for analysis of substrate, product and co-products. All experiments were carried out in duplicates.

Mycsp*AAO identification, sequence analysis, homology modelling and mutation design*

BLAST search within the genome of *Mycobacterium* sp. MS1601 was done using *Metsp*HMFO sequence as search query to find the putative oxidoreductases for HMF oxidation. The A0A1P8X5Y5 sequence was analysed using HAMMER server (Potter *et al.*, 2018). Multiple sequence alignment was done using PROMALS3D server (Pei *et al.*, 2008; Vinambres *et al.*, 2020). A maximum-likelihood phylogenetic tree was prepared by MEGA X software (Stecher *et al.*, 2020; Tamura *et al.*, 2021) applying 100-iteration bootstrapping (Felsenstein, 1985) using the Whelan and Goldman (2001) model of evolution.

The 3D structure for *Mycsp*AAO (A0A1P8X5Y5) was modelled using the Swiss-Model server, the nearest 12 templates in terms of coverage and sequence identities were used to build 12 models by the server (Pei *et al.*, 2008; Waterhouse *et al.*, 2018). The best model in terms of QMEAN score was eventually selected and was based on the template 2JBV, a choline oxidase that showed 38.9% sequence identity to *Mycsp*AAO (Quaye *et al.*, 2008; Benkert *et al.*, 2009). Another model was also built using YASARA Structure software and based solely on the template 3FIM, a fungal AAO to confirm the positions of the surface loop in front of the active site and the aromatic residues contributing to the active site. The FAD molecule was copied to the model and final energy minimization was performed using YASARA structure software (Krieger *et al.*, 2002). The docking analysis was carried out using AutoDock integrated into YASARA structure software and utilizing the macro dock_run.mer (Morris *et al.*, 2009). Molecular modelling was performed for 2 picoseconds using YASARA structure macro md_run.mer.

Cloning, expression and purification of Mycsp*AAO and its mutants*

*Mycsp*AAO gene was codon-optimized for expression in *E. coli* and tagged with a His-tag binding domain at the C-terminal end, and restriction sites for EcoRI and XhoI restriction enzymes were added to N-terminal and C-terminal, respectively (Fig. S1). The gene was synthesized at IDT (Integrated DNA Technologies, USA) and delivered in a pEX-K248 vector. pEX-K248-*Mycsp*AAO was co-digested with EcoRI and XhoI, and the desired gene fragment was ligated using T4 DNA Ligase to the expression vector pET-22b(+) that was co-digested with the same restriction enzymes. The plasmid was then transformed into *E. coli* DH5α, which was propagated in SOC medium for 60 min at 37°C, and grown on Luria-Bertani agar (Applichem, Darmstadt, Germany) in the presence of 100 μg ml^{-1} ampicillin. Plasmids were extracted from the resulting colonies and the correct clone was chosen after confirmation by colony PCR and sequencing (Eurofins Genomics, Germany), and the plasmid pET-22b(+)-*Mycsp*AAO was then transformed into chemically competent *E. coli* BL21 (DE3).

For expression of *Mycsp*AAO gene, 250 μl of an overnight culture of *E. coli* BL21 (DE3) cells bearing the pET-22b (+)-*Mycsp*AAO coding plasmid was transferred to 50 ml of Terrific Broth (TB) or NYAT medium containing 100 μg ml^{-1} ampicillin and grown at 37°C until reaching OD_{600} of 0.5. The cells were then induced with 1 mM IPTG and grown for 48 h at 15, 20 and 30°C, respectively, before harvesting by centrifugation at 4700 *g* for 15 min at 4°C (Sorvall LYNX 4000, Thermo Scientific, Germany). The cell pellet from 10 ml broth (OD_{600} nm of 5 adjusted for all samples) was re-suspended in 1 ml BugBuster™ Protein Extraction Reagent (Novagen, Germany) in 2 ml tubes and then incubated at 30°C for 15 min. Subsequently, all tubes were centrifuged for 30 min at 29 100 *g*, 4°C to separate the soluble and insoluble fractions. All subsequent steps were performed at 4°C. *Escherichia coli* BL21 (DE3) cells bearing the pET-22b (+) plasmid without the target gene were used as negative control. The soluble fraction was checked for *MycspAAO* expression by testing enzyme activity against 5-HMF and SDS-PAGE.

To purify the *Mycsp*AAO protein, the cells were cultured in 1L TB medium, induced with 1mM IPTG and incubated at 17°C for 48 h. The cell pellet was collected after centrifugation, lysed as mentioned above, and the protein was purified from the soluble fraction on 5 ml Ni-Sepharose™ High Performance, HisTrap™ HP column (GE-Healthcare) pre-equilibrated with the binding buffer of 50 mM sodium phosphate buffer and 40 mM imidazole. After washing the column, the bound protein was eluted with an elution buffer of 0.1 M phosphate buffer pH 7 supplemented with 500 mM imidazole. The eluted protein was dialysed against 50 mM phosphate buffer pH 8 using a dialysis membrane of 12–14 kDa molecular weight cutoff (Spectra/Por™, Thermo Fisher Scientific). The purified enzyme was used for further experiments.

The *Mycsp*AAO gene was transferred to pRSF-Duet plasmid with kanamycin resistance marker using the same restriction enzymes as indicated above. The target mutations were carried out using the designed primers (Table S2) and QuickChange™ site-directed mutagenesis kit. The PCR reaction of 50 μl contained 10 ng of template, 0.9 μl (125 ng) of primer pairs, 5 μl of 10× reaction buffer, 1 μl of dNTPs and 1 μl of Pfu ultra-DNA polymerase. The reaction was started at 95°C for 30 s for DNA template denaturation, followed by 16 amplification cycles, each of which involved 95°C for 30 s, 55°C for 1 min and 68°C for 5 min for template denaturation, annealing and extension, respectively. The PCR products were mixed gently with 1 μl of DpnI and incubated for 1 h at 37°C and then the products were analysed by gel electrophoresis. Thereafter, 2 μl of the DpnI treated PCR products were transformed into *E. coli* One Shot Top10 using heat shock and then placed on ice for 30 min.

The transformed cells were propagated in SOC medium for 1 h at 37°C and 225 rpm and then plated on LB agar supplemented with 50 μg ml^{-1} kanamycin and incubated overnight at 37°C. The colonies obtained were sub-cultured on LB broth supplemented with 50 μg ml^{-1} kanamycin. The plasmids with wild-type and mutant *Mycsp*AAO were purified using Qiagen miniprep kits (Qiagen, Hilden, Germany) and used for PCR analysis using the corresponding primer pairs for further confirmation. Moreover, the mutations were confirmed by DNA sequencing (Eurofins, Hamburg, Germany). The plasmids with successful mutations were transformed into *E. coli* BL21 (DE3) competent cells, which were cultivated overnight at 37°C in LB medium with 50 μg ml^{-1} kanamycin. The cells were then suspended in 20% glycerol and stored at −80°C for further use.

Expression of wild-type and mutant *Mycsp*AAO genes was carried out in 50 ml TB medium containing 50 μg ml^{-1} kanamycin. The cells were grown at 37°C until reaching OD_{600} of 0.5 and then induced with 1 mM IPTG, after which the cell growth was continued for 72 h at 17°C. The cells were harvested and lysed as described above. Twenty microlitre supernatant was used for SDS-PAGE, and 200 μl was added to 800 μl of 0.1 M phosphate buffer pH 8 in a total volume of 1 ml containing 2.5 mM HMF, for the activity tests. *Mycsp*AAO, *Mycsp*AAO-Y444F and *Mycsp*AAO-L298A exhibiting relatively higher activity against HMF were chosen for production in 1L of TB medium and

purification of the enzymes was carried out as mentioned above. The purified enzymes after desalting were stored in 40% glycerol at −20°C for further screening and application.

The homogeneity of the purified protein was confirmed by SDS-PAGE using 12% (w/v) separating gel and 3% (w/v) stacking gel (Laemmli, 1970). The protein concentration was determined using a BCA assay kit with bovine serum albumin as standard following the manufacturer's instructions.

Substrate spectrum and optimum conditions for activity and of Mycsp*AAO*

Activity of pure *Mycsp*AAO against HMF (4 mM; 0.5 g l^{-1}) was determined using 40 μg ml^{-1} enzyme in 200 μl of 100 mM sodium phosphate buffer pH 8 in 1.5 ml Eppendorf tubes and incubation at 30°C and 500 rpm in a thermoshaker (MKR 13, HLC Biotech, Germany) for 2 h. The concentrations of substrate and product(s) were determined by HPLC. For determining optimum pH, the reaction was performed in 100 mM phosphate buffer pH 5, 6, 7, 8 and 9, respectively, at 30°C while maintaining the other conditions as above. The optimum temperature of the HMF oxidizing activity was determined by varying the reaction temperature between 20–70°C. The optimum conditions of pH and incubation temperature were then applied for oxidation of 4 mg ml^{-1} HMF using 40 μg pure *Mycsp*AAO in 1 ml of 100 mM phosphate buffer in 4 ml vials, incubated at 30°C and 700 rpm in a thermomixer for 48 h. All experiments were carried out in duplicates.

The activity and specific activity of the pure *Mycsp*AAO was also tested against 5 mM of different substrates besides HMF, including furfural, FFCA, DFF, BHMF, HMFCA, 4-hydroxy benzyl alcohol (4-HBA), benzyl alcohol (BA), n-propanol (n-P-OL), veratryl alcohol (3,4 di-methoxy benzyl alcohol, 3,4DMBA), methoxy benzyl alcohol (MBA), choline, pyridoxine, glycerol, methanol and glucose, using 20 μl of the enzyme solution (protein concentration of 8 μg ml^{-1}) in 200 μl total reaction volume in a microtitre plate. The assay was performed at pH 8 and 30°C as a coupled assay in which H_2O_2 generated in the oxidation reaction is used by horseradish peroxidase (HRP, 15 U ml^{-1}) to oxidize 4-aminoantipyrine (0.1 mM) and 3,5-dichloro-2-hydroxybenzensulfonic acid (1 mM) to form a pink product that is detected at 515 nm (Dijkman and Fraaije, 2014) in a spectrophotometer (Multiskan Go, Thermo Fisher Scientific, Sweden). Blank reactions corresponding to each substrate without enzyme were included as negative controls. The assay was also used to determine the specific activity of *Mycsp*AAO and *Mycsp*AAO-Y444F against HMF, furfural, 4-HBA, glucose, glycerol, choline, pyridoxine and methanol.

Calculations of activity, yield and kinetic analysis

The activity and specific activity of the wild-type *Mycsp*AAO against different substrates was calculated using the following equations

$$\text{Activity} = \frac{\left(\frac{\text{Sample }(A515)}{t} - \frac{\text{Blank }(A515)}{t}\right) * \text{total reaction volume (ml)} * \text{dilution factor}}{\text{enzyme volume} \times \epsilon} = U\left(\frac{\mu\text{mole}}{\text{min}}\right)/\text{ml} \quad (1)$$

$$\text{Specific activity} = \frac{\text{U/ml}}{\text{total protein conc. } \left(\frac{\text{mg}}{\text{ml}}\right)} = U\left(\frac{\mu\text{mole}}{\text{min}}\right)/\text{mg} \quad (2)$$

The product yield ($Y_{p/s}$) and selectivity (S) were calculated using the following equations:

$$Y_{p/s}(\%) = [(\text{Product}_{\text{final}} - \text{Product}_{\text{initial}}) / (\text{Substrate}_{\text{initial}} - \text{Substrate}_{\text{final}})] \times 100$$

$$S(\%) = [\text{Product (moles)} - \text{byproducts (moles)} / \text{converted HMF (moles)}] \times 100$$

The kinetic parameters, V_{max}, K_m, k_{cat} and k_{cat}/K_m for *Mycsp*AAO, *Mycsp*AAO-Y444F and *Mycsp*AAO-L298A were determined by Lineweaver–Burk plot with data from the reactions with 0.1–80 mM HMF as substrate using 10 μg ml^{-1} of the purified enzyme variants in 200 μl total reaction volume of 100 mM sodium phosphate buffer pH 8 at 30°C for 3 h. Fifty microlitre samples were collected every 30 min and the slope of the linear relation between HMF concentration (mM) and time was used to calculate the reaction rate (V). Both V_{max} and K_m were obtained directly from Lineweaver–Burk plot and k_{cat} was calculated according to the following equation $k_{cat} = V_{max}/[E]_0$ where $[E]_0$ is the initial enzyme concentration (mM).

The activities of pure *Mycsp*AAO-WT and *Mycsp*AAO-Y444F were compared for oxidation of HMF by mixing 200 μl enzyme solutions (1 mg ml^{-1}) with 0.8 ml of 10 mM HMF in 0.1 mM sodium phosphate buffer pH 8 in 4 ml vials, incubating in a thermoshaker at 30°C and

500 rpm and collecting 20 μl samples at regular time intervals for HPLC analysis.

Analytical procedures

The concentrations of 5-HMF, FFA, FFCA and FDCA were determined using HPLC (JASCO, Tokyo, Japan) equipped with a fast acid analysis chromatographic column connected to a guard column (Biorad, Richmond, CA, USA), refractive index detector (ERC, Kawaguchi, Japan), a JASCO UV detector operating at 215 nm and a JASCO intelligent autosampler. The column temperature was maintained at 65°C in a chromatographic oven (Shimadzu, Tokyo, Japan). Samples were diluted with Milli-Q quality water and mixed with 20% (v/v) H_2SO_4 (20 μl ml^{-1} sample) and then filtered. A 40 μl aliquot was injected in 0.5 mM H_2SO_4 mobile phase flowing at a rate of 0.4 ml min^{-1}. The peaks for the different compounds were confirmed and quantified using the corresponding external standards.

To determine the FAD bound to the enzyme, 500 μl of 1 mg ml^{-1} of pure *Mycsp*AAO-WT was filtered using 30 kDa cut-off and washed twice using 500 μl of 0.1 M phosphate buffer pH 8, and then denatured at 100°C for 15 min and separated by centrifugation at 15 000 *g* for 5 min. The released FAD was detected at 450 nm in a spectrophotometer (Boateng *et al*., 2015, Dishisha *et al*., 2019), and the concentration was calculated based on a standard curve.

Acknowledgements

The authors gratefully acknowledge the financial support from the Swedish Foundation for Strategic Environmental Research (Mistra) for the research program, Sustainable Plastics and Transition Pathways (STEPS) (grant no. 2016/1489) and the Swedish Research Council FORMAS (grant no. 942-2016-33) for the project Farm2-Furan at Lund University.

Conflict of interest

The authors declare no conflict of interest.

Author contributions

RHK and MS conceptualized the work. MS and RHK planned the experiments. MS designed and carried out the experiments and the analysis. YG designed and performed the *in silico* analyses. FJ helped with the mutagenesis experiments and EVM with the experiments on characterization of the wild-type enzyme. MS, RHK, SHP and YG were involved in writing and revising the manuscript.

References

Aleksenko, V.A., Anand, D., Remeeva, A., Nazarenko, V.V., Gordeliy, V., Jaeger, K.-E., *et al*. (2020) Phylogeny and structure of fatty acid photodecarboxylases and glucose-methanol-choline oxidoreductases. *Catalysts* **10:** 1072.

Benkert, P., Künzli, M., and Schwede, T. (2009) QMEAN server for protein model quality estimation. *Nucl Acids Res* **37(suppl 2):** W510–W514.

Boateng, M.O., Corrigall, A.V., Sturrock, E., and Meissner, P.N. (2015) Characterisation of the flavin adenine dinucleotide binding region of *Myxococcus xanthus* protoporphyrinogen oxidase. *Biochem Biophys Rep* **4:** 306–311.

Bozell, J.J., and Petersen, G.R. (2010) Technology development for the production of biobased products from biorefinery carbohydrates—the US Department of Energy's "Top 10" revisited. *Green Chem* **12:** 539–554.

Carro, J., Amengual-Rigo, P., Sancho, F., Medina, M., Guallar, V., Ferreira, P., and Martinez, A.T. (2018a) Multiple implications of an active site phenylalanine in the catalysis of aryl-alcohol oxidase. *Sci Rep* **8:** 8121.

Carro, J., Fernández-Fueyo, E., Fernández-Alonso, C., Cañada, J., Ullrich, R., Hofrichter, M., *et al*. (2018b) Self-sustained enzymatic cascade for the production of 2,5-furandicarboxylic acid from 5-methoxymethylfurfural. *Biotechnol Biofuels* **11:** 1–10.

Carro, J., Ferreira, P., Rodríguez, L., Prieto, A., Serrano, A., Balcells, B., *et al*. (2015) 5-hydroxymethylfurfural conversion by fungal aryl-alcohol oxidase and unspecific peroxygenase. *FEBS J* **282:** 3218–3229.

Cavener, D.R. (1992) GMC oxidoreductases: a newly defined family of homologous proteins with diverse catalytic activities. *J Mol Biol* **223:** 811–814.

Chadderdon, D.J., Xin, L., Qi, J., Qiu, Y., Krishna, P., More, K.L., and Li, W. (2014) Electrocatalytic oxidation of 5-hydroxymethylfurfural to 2, 5-furandicarboxylic acid on supported Au and Pd bimetallic nanoparticles. *Green Chem* **16:** 3778–3786.

Chakraborty, M., Goel, M., Chinnadayyala, S.R., Dahiya, U.R., Ghosh, S.S., and Goswami, P. (2014) Molecular characterization and expression of a novel alcohol oxidase from *Aspergillus terreus* MTCC6324. *PLoS One* **9:** e95368.

Chen, G., van Straalen, N.M., and Roelofs, D. (2016) The ecotoxicogenomic assessment of soil toxicity associated with the production chain of 2, 5-furandicarboxylic acid (FDCA), a candidate bio-based green chemical building block. *Green Chem* **18:** 4420–4431.

Davidson, M.G., Elgie, S., Parsons, S., and Young, T.J. (2021) Production of HMF, FDCA and their derived products: a review of life cycle assessment (LCA) and techno-economic analysis (TEA) studies. *Green Chem* **23:** 3154–3171.

Dijkman, W.P. (2015) HMF oxidase: characterization, application and engineering of 5-(hydroxymethyl)furfural oxidase. PhD Thesis. Groningen, the Netherlands: University of Groningen.

Dijkman, W.P., Binda, C., Fraaije, M.W., and Mattevi, A. (2015) Structure-based enzyme tailoring of 5-hydroxymethylfurfural oxidase. *ACS Catal* **5:** 1833–1839.

Dijkman, W.P., and Fraaije, M.W. (2014) Discovery and characterization of a 5-hydroxymethylfurfural oxidase from

Methylovorus sp. strain MP688. *Appl Environ Microbiol* **80:** 1082–1090.

Dijkman, W.P., Groothuis, D.E., and Fraaije, M.W. (2014) Enzyme-catalyzed oxidation of 5-hydroxymethylfurfural to furan-2,5-dicarboxylic acid. *Angew Chem Int Ed* **53:** 6515–6518.

Dishisha, T., Sabet-Azad, R., Arieta, V., and Hatti-Kaul, R. (2019) *Lactobacillus reuteri* NAD (P) H oxidase: properties and coexpression with propanediol-utilization enzymes for enhancing 3-hydroxypropionic acid production from 3-hydroxypropionaldehyde. *Journal of biotechnology* **289:** 135–143.

Felsenstein, J. (1985) Confidence limits on phylogenies: an approach using the bootstrap. *Evolution* **39:** 783–791.

Ferreira, P., Hernández-Ortega, A., Herguedas, B., Rencoret, J., Gutiérrez, A., Martínez, M.J., *et al*. (2010) Kinetic and chemical characterization of aldehyde oxidation by fungal aryl-alcohol oxidase. *Biochem J* **425:** 585–593.

Ferreira, P., Hernández-Ortega, A., Lucas, F., Carro, J., Herguedas, B., Borrelli, K.W., *et al*. (2015) Aromatic stacking interactions govern catalysis in aryl-alcohol oxidase. *FEBS J* **282:** 3091–3106.

Galperin, I., Javeed, A., Luig, H., Lochnit, G., and Rühl, M. (2016) An aryl-alcohol oxidase of *Pleurotus sapidus*: heterologous expression, characterization, and application in a 2-enzyme system. *Appl Microbiol Biotechnol* **100:** 8021–8030.

Hernandez-Ortega, A., Lucas, F., Ferreira, P., Medina, M., Guallar, V., and Martinez, A.T. (2011) Modulating O_2 reactivity in a fungal flavoenzyme: involvement of aryl-alcohol oxidase Phe-501 contiguous to catalytic histidine. *J Biol Chem* **286:** 41105–41114.

Jankowski, N., Koschorreck, K., and Urlacher, V.B. (2020) High-level expression of aryl-alcohol oxidase 2 from *Pleurotus eryngii* in *Pichia pastoris* for production of fragrances and bioactive precursors. *Appl Microbiol Biotechnol* **104:** 9205–9218.

Kawde, A., Sayed, M., Shi, Q., Uhlig, J., Pullerits, T., and Hatti-Kaul, R. (2021) Photoelectrochemical oxidation in ambient conditions using earth-abundant hematite anode: a green route for the synthesis of biobased polymer building blocks. *Catalysts* **11:** 969.

Krieger, E., Koraimann, G., and Vriend, G. (2002) Increasing the precision of comparative models with YASARA NOVA—a self-parameterizing force field. *Proteins: Struct Func Bioinform* **47:** 393–402.

Laemmli, U.K. (1970) Cleavage of structural proteins during the assembly of the head of bacteriophage T4. *Nature* **227:** 680–685.

Lappe, A., Jankowski, N., Albrecht, A., and Koschorreck, K. (2021) Characterization of a thermotolerant aryl-alcohol oxidase from *Moesziomyces antarcticus* oxidizing 5-hydroxymethyl-2-furancarboxylic acid. *Appl Microbiol Biotechnol* **105:** 8313–8327.

McKenna, S.M., Leimkühler, S., Herter, S., Turner, N.J., and Carnell, A.J. (2015) Enzyme cascade reactions: synthesis of furandicarboxylic acid (FDCA) and carboxylic acids using oxidases in tandem. *Green Chem* **17:** 3271–3275.

McKenna, S.M., Mines, P., Law, P., Kovacs-Schreiner, K., Birmingham, W.R., Turner, N.J., *et al*. (2017) The continuous oxidation of HMF to FDCA and the immobilisation and stabilisation of periplasmic aldehyde oxidase (PaoABC). *Green Chem* **19:** 4660–4665.

Morris, G.M., Huey, R., Lindstrom, W., Sanner, M.F., Belew, R.K., Goodsell, D.S., *et al*. (2009) AutoDock4 and AutoDockTools4: automated docking with selective receptor flexibility. *J Comput Chem* **30:** 2785–2791.

Pei, J., Kim, B.-H., and Grishin, N.V. (2008) PROMALS3D: a tool for multiple protein sequence and structure alignments. *Nucleic Acids Res* **36:** 2295–2300.

Potter, S.C., Luciani, A., Eddy, S.R., Park, Y., Lopez, R., and Finn, R.D. (2018) HMMER web server: 2018 update. *Nucleic Acids Res* **46:** W200–W204.

Pyo, S.-H., Park, J.H., Srebny, V., and Hatti-Kaul, R. (2020) A sustainable synthetic route for biobased 6-hydroxyhexanoic acid, adipic acid and ε-caprolactone by integrating bio-and chemical catalysis. *Green Chem* **22:** 4450–4455.

Quaye, O., Lountos, G.T., Fan, F., Orville, A.M., and Gadda, G. (2008) Role of Glu312 in binding and positioning of the substrate for the hydride transfer reaction in choline oxidase. *Biochemistry* **47:** 243–256.

Ribeiro, M.L., and Schuchardt, U. (2003) Cooperative effect of cobalt acetylacetonate and silica in the catalytic cyclization and oxidation of fructose to 2,5-furandicarboxylic acid. *Catal Commun* **4:** 83–86.

Sajid, M., Zhao, X., and Liu, D. (2018) Production of 2,5-furandicarboxylic acid (FDCA) from 5-hydroxymethylfurfural (HMF): recent progress focusing on the chemical-catalytic routes. *Green Chem* **20:** 5427–5453.

Sánchez-Ruiz, M.I., Martínez, A.T., and Serrano, A. (2021) Optimizing operational parameters for the enzymatic production of furandicarboxylic acid building block. *Microb Cell Fact* **20:** 1–13.

Savino, S., and Fraaije, M.W. (2021) The vast repertoire of carbohydrate oxidases: an overview. *Biotechnol Adv* **51:** 107634.

Sayed, M., Dishisha, T., Sayed, W.F., Salem, W.M., Temerk, H.A., and Pyo, S.-H. (2016) Selective oxidation of trimethylolpropane to 2, 2-bis (hydroxymethyl) butyric acid using growing cells of *Corynebacterium* sp. ATCC 21245. *J Biotechnol* **221:** 62–69.

Sayed, M., Dishisha, T., Sayed, W.F., Salem, W.M., Temerk, H.M., and Pyo, S.-H. (2017a) Enhanced selective oxidation of trimethylolpropane to 2,2-bis (hydroxymethyl) butyric acid using *Corynebacterium* sp. ATCC 21245. *Process Biochem* **63:** 1–7.

Sayed, M., Sayed, W.F., Hatti-Kaul, R., and Pyo, S.-H. (2017b) Complete genome sequence of *Mycobacterium* sp. MS1601, a bacterium performing selective oxidation of polyols. *Genome Announc* **5:** e00156-00117.

Sayed, M., Warlin, N., Hulteberg, C., Munslow, I., Lundmark, S., Pajalic, O., *et al*. (2020) 5-Hydroxymethylfurfural from fructose: An efficient continuous process in a water-dimethyl carbonate biphasic system with high yield product recovery. *Green Chem* **22:** 5402–5413.

Serrano, A., Calviño, E., Carro, J., Sánchez-Ruiz, M.I., Cañada, F.J., and Martínez, A.T. (2019) Complete oxidation of hydroxymethylfurfural to furandicarboxylic acid by aryl-alcohol oxidase. *Biotechnol Biofuels* **12:** 1–12.

Serrano, A., Carro, J., and Martínez, A.T. (2020) Reaction mechanisms and applications of aryl-alcohol oxidase. In

Enzymes. Chaiyen, P., and Tamanoi, F. (eds). Amsterdam, the Netherlands: Elsevier, pp. 167–192.
Sousa, A.F., Coelho, J.F.J., and Silvestre, A.J.D. (2016) Renewable-based poly((ether)ester)s from 2,5-furandicarboxylic acid. *Polymer* **98:** 129–135.
Sousa, A.F., Vilela, C., Fonseca, A.C., Matos, M., Freire, C.S.R., Gruter, G.-J., *et al*. (2015) Biobased polyesters and other polymers from 2,5-furandicarboxylic acid: a tribute to furan excellency. *Polym Chem* **6:** 5961–5983.
Stecher, G., Tamura, K., and Kumar, S. (2020) Molecular evolutionary genetics analysis (MEGA) for macOS. *Mol Biol Evol* **37:** 1237–1239.
Sützl, L., Foley, G., Gillam, E.M., Bodén, M., and Haltrich, D. (2019) The GMC superfamily of oxidoreductases revisited: analysis and evolution of fungal GMC oxidoreductases. *Biotechnol Biofuels* **12:** 1–18.
Sützl, L., Laurent, C.V., Abrera, A.T., Schütz, G., Ludwig, R., and Haltrich, D. (2018) Multiplicity of enzymatic functions in the CAZy AA3 family. *Appl Microbiol Biotechnol* **102:** 2477–2492.
Tamboli, D.P., Telke, A.A., Dawkar, V.V., Jadhav, S.B., and Govindwar, S.P. (2011) Purification and characterization of bacterial aryl alcohol oxidase from *Sphingobacterium* sp. ATM and its uses in textile dye decolorization. *Biotechnol Bioproc Eng* **16:** 661–668.
Tamura, K., Stecher, G., and Kumar, S. (2021) MEGA11: molecular evolutionary genetics analysis version 11. *Mol Biol Evol* **38:** 3022–3027.
Troiano, D., Orsat, V., and Dumont, M.-J. (2020) Status of biocatalysis in the production of 2, 5-furandicarboxylic acid (FDCA). *ACS Catal* **10:** 9145–9169.
Urlacher, V.B., and Koschorreck, K. (2021) Pecularities and applications of aryl-alcohol oxidases from fungi. *Appl Microbiol Biotechnol* **105:** 4111–4126.
Viña-Gonzalez, J., Martinez, A.T., Guallar, V., and Alcalde, M. (2020) Sequential oxidation of 5-hydroxymethylfurfural to furan-2,5-dicarboxylic acid by an evolved aryl-alcohol oxidase. *Biochim Biophys Acta* **1868:** 140293. https://doi.org/10.1016/j.bbapap.2019.140293
Vinambres, M., Espada, M., Martinez, A.T., and Serrano, A. (2020) Screening and evaluation of new hydroxymethylfurfural oxidases for furandicarboxylic acid production. *Appl Environ Microbiol* **86:** e00842-20. https://doi.org/10.1128/AEM.00842-20
Waterhouse, A., Bertoni, M., Bienert, S., Studer, G., Tauriello, G., Gumienny, R., *et al*. (2018) SWISS-MODEL: homology modelling of protein structures and complexes. *Nucl Acids Res* **46:** W296–W303.
Werpy, T., Petersen, G., Aden, A., Bozell, J., Holladay, J., White, J., *et al*. (2004) *Top Value Added Chemicals from Biomass. Volume 1-Results of Screening for Potential Candidates from Sugars and Synthesis Gas*. Washington, DC, USA: Department of Energy.
Whelan, S., and Goldman, N. (2001) A general empirical model of protein evolution derived from multiple protein families using a maximum-likelihood approach. *Mol Biol Evol* **18:** 691–699.
Yuan, H., Li, J., Shin, H.-D., Du, G., Chen, J., Shi, Z., and Liu, L. (2018) Improved production of 2,5-furandicarboxylic acid by overexpression of 5-hydroxymethylfurfural oxidase and 5-hydroxymethylfurfural/furfural oxidoreductase in *Raoultella ornithinolytica* BF60. *Bioresour Technol* **247:** 1184–1188.
Yuan, H., Liu, H., Du, J., Liu, K., Wang, T., and Liu, L. (2020) Biocatalytic production of 2,5-furandicarboxylic acid: recent advances and future perspectives. *Appl Microbiol Biotechnol* **104:** 527–543.
Zhang, J., Li, J., Tang, Y., Lin, L., and Long, M. (2015) Advances in catalytic production of bio-based polyester monomer 2, 5-furandicarboxylic acid derived from lignocellulosic biomass. *Carbohyd Polym* **130:** 420–428.
Zhang, Z., and Deng, K. (2015) Recent advances in the catalytic synthesis of 2,5-furandicarboxylic acid and its derivatives. *ACS Catal* **5:** 6529–6544.

Supporting information

Additional supporting information may be found online in the Supporting Information section at the end of the article.

Fig. S1. Sequence analysis of A0A1P8X5Y5 (*Mycsp*AAO). A) BLAST search of the sequence in the UniProt database, the retrieved 250 hits did not show any biochemically characterized protein. B) A0A1P8X5Y5 in red color was aligned with the characterized protein found in the CAZY AA3 proteins and it was clustered within the AA3_2 subfamily. AA3_1 subfamily sequences are colored green, AA3_2 subfamily are colored blue, AA3_3 are colored black, and AA3_4 are colored pink. C) A screenshot shows part of the whole alignment of A0A1P8X5Y5, highlighted in coral color, against 4220 fungal GMC oxidoreductases that have been recently classified into 5 clusters by Sützl et al. The A0A1P8X5Y5 was aligned under the A0A0H2S5F3, a putative aryl-alcohol oxidase from *Schizopora paradoxa* and within the AAO–PDH cluster according to Sützl et al (2019). Catalytic histidine is highlighted yellow, with the highest conservancy score (9). D) Comparison to characterized AAOs from fungal sources from *Pleurotus eryngii*, *Pleurotus sapidus* and *Thermothelomyces thermophilus*. The multiple sequence alignment was done using PROMALS3D server.

Fig. S2. Nucleotide sequence of *Mycsp*AAO optimized gene for expression in *E. coli*.

Fig. S3. Comparison of *Mycsp*AAO described in the current study to the HMFOs characterized in literature, *Metsp*HMFO, *Pseni*HMFO, and *Psesp*HMFO. The numbered boxes show the positions where *Mycsp*AAO differs compared to the three HFMOs, the yellow highlighted sequence parts show the ADP-binding motif, PS000623 and PS000624 motifs. The table shows the specific differences in *Mycsp*AAO compared to the three HMFOs. Code for the alignment: secondary structure predictions (red: alpha-helix, blue: beta-strand). Consensus predicted secondary structure symbols: alpha-helix: h; beta-strand: e. Consensus amino acid symbols: conserved amino acids are in bold and uppercase letters; aliphatic (I, V, L): l; aromatic (Y, H, W, F): @; hydrophobic (W, F, Y, M, L, I, V, A, C, T, H): h; alcohol (S, T): o; polar residues (D, E, H, K, N, Q, R, S, T): p; tiny (A, G, C, S): t; small (A, G, C, S, V, N, D, T, P): s; bulky residues (E, F, I, K, L, M, Q, R, W, Y): b; positively charged (K,

R, H): +; negatively charged (D, E): -; charged (D, E, K, R, H): c. The figure is created using PROMALS3D.

Fig. S4. Conversion of HMF (4 mM) using the soluble fraction containing *Mycsp*AAO-WT from *Mycobacterium* sp. MS1601 expressed in *E. coli* BL21 (DE3) at 15, 20, and 30 °C, respectively, in (A) NYAT and (B) TB media. The experimental details are described in the text.

Fig. S5. The colorimetric assay results of MycspAAO-WT and -Y444F for the oxidation of 5 mM of different substrates after 30 min reaction time.

Fig. S6. Overall view of the homology model constructed for MycspAAO.

Fig. S7. A) Ramachandran plot for MycspAAO, B) Z-score of the homology model MycspAAO (UniProt accession code: A0A1P8X5Y5). The Z-score is < 1, indicating a good model.

Fig. S8. The possible catalytic binding mode of the substrate HMF in the active site of *Mycsp*AAO 3D model (A) based on the docking experiments. The hydroxyl moiety of HMF is at hydrogen bond distance to the catalytic H445 and is probably stabilized by hydrogen bonding to Q335. The amino acids V95, L97, M337, N487, Y444, Y443, A317 are shaping the active site and are probably critical for substrate selectivity. T356 is a candidate for mutation because of its proximity to the substrate-binding site. (B) Another pose of the HMF in the active site that was detected in the docking experiments. The substrates (either 5-HMF or hydrated 5-HMF) are possibly involved in hydrogen bonding with Y444 that misorient the oxidizable Cα of the substrate against the N5-FAD atom. Mutating Y444 into F showed improved enzymatic activity.

Fig. S9. SDS- PAGE representing the purification of MycspAAO: wild type (WT), and variants Y444F, and L298A expressed in E. coli BL21 (DE3).

Fig. S10. Initial reaction rate of HMF oxidation at different concentrations using Mycsp AAO variants. The reaction was carried out at pH 8 and 30 °C for 3 hours. HMF and FFCA concentrations were measured by HPLC.

Fig. S11. Screening of the activity of purified wild type *Mycsp*AAO-WT (red) and *Mycsp*AAO-Y444F (blue) (8 μg/mL of total protein) for the oxidation of different substrates used at 5 mM concentration, pH 8, and 30 °C using the colorimetric coupled assay with horseradish peroxidase.

Table S1. Proposed mutations for *Mycsp*AAO, and their expected outcomes. The mutations that were not successfully obtained are marked with an asterix.

Table S2. List of primers used for site-directed mutagenesis.

Table S3. Protein concentrations of wild type *Mycsp*AAO and variants based on BCA assay, used for determination of activity with HMF.

